Vol 17 No 3, March 2008
1674-1056/2008/17(03)/0883-13

Chinese Physics B

© 2008 Chin. Phys. Soc.
and IOP Publishing Ltd

Anisotropic emission of charged mesons and structure characteristic of emission source in heavy ion collisions at 1–2A GeV*

Liu Fu-Hu(刘福虎)†

Institute of Theoretical Physics, Shanxi University, Taiyuan 030006, *China*

(Received 10 May 2007; revised manuscript received 10 September 2007)

Angular distributions of pions and kaons produced in heavy ion collisions at the low-energy end of high energies (1–2 A GeV) have been investigated by using a multisource ideal gas model. The model covers the expansions and movements of the emission sources, and it is related to the collective flows. By using the analytic expression and the Monte Carlo method, the azimuthal and polar angle distributions of mesons are calculated by the model and compared with the experimental data of the KaoS Collaboration.

Keywords: low-energy end of high energies, heavy ion collisions, charged mesons, anisotropic emission

PACC: 2500, 2570, 1440D, 1440F

1. Introduction

Heavy ion collisions at high energies provide a unique opportunity to investigate both the multiparticle production and the multifragment emission process. In particular, 1–2 A GeV is considered to be at low-energy end of high energies. In the intermediate energy (MeV) region and the high energy (GeV) region, the mechanisms of nuclear reactions are expected to be different from each other.

There are a few accelerators working at the low-energy and of high energies. For example, the Bevalac at the Lorentz Berkeley Laboratory (LBL) in Berkeley and the heavy ion synchrotron (SIS) at the Gesellschaft für Schwerionenforschung mbH (GSI) in Darmstadt can accelerate heavy ions to 1–2 A GeV,[1] the Synchrophasotron at the Joint Institute for Nuclear Research (JINR) in Dubna to $3-5$ A GeV,[2] and the Alternating–Gradient Synchrotron (AGS) at the Brookhaven National Laboratory (BNL) in Brookhaven to energies ranging from 2 A to 15 A GeV.[3] It is expected that the Cooling Storage Ring (CSR) at the Heavy Ion Research Facility in Lanzhou (HIRFL) and the Institute of Modern Physics (IMP) in Lanzhou will accelerate heavy ions to a few A GeV or lower energies.[4]

In higher energy regions, the Super Proton Synchrotron (SPS) at the European Organization for Nuclear Research (CERN) in Geneva can accelerate heavy ions to energies ranging from 20 A to 200A GeV.[5] In ultrahigh energy regions, the Relativistic Heavy Ion Collider (RHIC) at BNL in Brookhaven has been working in a centre-of-mass energy range from 22.5 A to 200 A GeV since June 2000,[6] and the Large Hadron Collider (LHC) at CERN in Geneva is expected to work in a centre-of-mass energy range from 5.5 A to 14 A TeV in the near future.[7]

Many experimental results of heavy ion collisions at high energies have been reported in the past 20–30 years.[8−12] Meanwhile, more theoretical models have been suggested to explain the experimental results.[13−23] To describe the multifragment emission process, we have suggested a multisource ideal gas model and explained the azimuthal and polar angle distributions of fragments produced in the projectile and target nuclei in an energy range covering the energies achieved by AGS and SPS by using the Monte Carlo method.[24−27]

To give a further test to the multisource ideal gas

*Project supported by the National Natural Science Foundation of China (Grant Nos 10675077 and 10275042), the Shanxi Provincial Natural Science Foundation of China (Grant No 2007011005), and the Shanxi Provincial Foundation for Returned Overseas Scholars, China.

†E-mail: fuhuliu@163.com

model, in this paper, we study the angular distributions of pions and kaons produced in heavy ion collisions at 1–2 A GeV. Not only the Monte Carlo method but also the analytic expression is given in the present paper. The calculated results are compared with the experimental data of the KaoS Collaboration.[28−32]

2. The model and formulation

The model used in this paper is called the multi-source ideal gas model which can be found in our previous work.[24−27] Only the Monte Carlo method was introduced in the previous work. The analytic expression was lacking due to our insufficient knowledge at that time. Now we describe the model by using both the analytic expression and the Monte Carlo method in the present work.

To describe the model, let the beam travel along the oz-axis and the reaction plane be the yoz-plane. Many emission sources of particles (or fragments) are assumed to be formed in participant (or spectator) in high energy heavy ion collisions. Each emission source is treated as an ideal gas source. The interactions among different emission sources affect the emissions of particles (or fragments).

In the rest frame of the emission source, as used in a Maxwell's ideal gas model, the three components p'_x, p'_y, and p'_z of momentum of particle (or fragment) concerned obey the Gaussian distribution and have the same standard deviation σ,

$$f_{p'_{x,y,z}}(p'_{x,y,z}) = \frac{1}{\sqrt{2\pi}\sigma}\exp\left(-\frac{p'^2_{x,y,z}}{2\sigma^2}\right). \tag{1}$$

Considering the interactions among different emission sources, the source concerned will have expansions and movements in the momentum space. Due to the expansions and movements of the source concerned in the momentum space, the momentum components p_x, p_y, and p_z of the momentum of particle (or fragment) concerned in a final state will depart from the Gaussian distribution. We need two kinds of parameters to describe the effects of the expansions and movements of the source concerned separately. Let $B_{x,y,z}$ represent the movements and $a_{x,y,z}$ and $b_{x,y,z}$ denote the coefficients which describe the effects of the expansions and movements of the source respectively. The simplest relation between the momentum in source rest frame and the momentum in final state is linear. We have

$$\begin{aligned} p_{x,y,z} &= a_{x,y,z}p'_{x,y,z} + B_{x,y,z} \\ &= a_{x,y,z}p'_{x,y,z} + b_{x,y,z}\sigma. \end{aligned} \tag{2}$$

It seems that Eq.(2) is in contradiction with the Lorentz transformation. We point out that one could understand the current formalism because Eq.(2) represents the relations between 'mean' momenta in the cases of laboratory (or centre-of-mass) reference frame and source rest frame. According to the knowledge of probability theory and Eq.(2), the distributions of $p_{x,y,z}$ can be given by

$$\begin{aligned} & f_{p_{x,y,z}}(p_{x,y,z}) \\ &= \frac{1}{\sqrt{2\pi}\sigma a_{x,y,z}} \\ &\quad \times \exp\left[-\frac{1}{2\sigma^2}\left(\frac{p_{x,y,z} - b_{x,y,z}\sigma}{a_{x,y,z}}\right)^2\right]. \end{aligned} \tag{3}$$

The unit-density functions of p_x and p_y are

$$\begin{aligned} & f_{p_x,p_y}(p_x,p_y) \\ &= f_{p_x}(p_x)f_{p_y}(p_y) \\ &= \frac{1}{2\pi\sigma^2 a_x a_y}\exp\left[-\frac{1}{2\sigma^2}\left(\frac{p_x - b_x\sigma}{a_x}\right)^2\right. \\ &\quad \left.-\frac{1}{2\sigma^2}\left(\frac{p_y - b_y\sigma}{a_y}\right)^2\right]. \end{aligned} \tag{4}$$

Considering the transverse momentum

$$p_{\rm T} = \sqrt{p_x^2 + p_y^2}, \tag{5}$$

and the azimuthal angle

$$\varphi = \arctan\frac{p_y}{p_x}, \tag{6}$$

we have the unit-density functions of $p_{\rm T}$ and φ as

$$\begin{aligned} & f_{p_{\rm T},\varphi}(p_{\rm T},\varphi) \\ &= p_{\rm T} f_{p_x,p_y}(p_{\rm T}\cos\varphi, p_{\rm T}\sin\varphi) \\ &= \frac{p_{\rm T}}{2\pi\sigma^2 a_x a_y}\exp\left[-\frac{1}{2\sigma^2}\left(\frac{p_{\rm T}\cos\varphi - b_x\sigma}{a_x}\right)^2\right. \\ &\quad \left.-\frac{1}{2\sigma^2}\left(\frac{p_{\rm T}\sin\varphi - b_y\sigma}{a_y}\right)^2\right]. \end{aligned} \tag{7}$$

Thus, the $p_{\rm T}$ distribution is

$$f_{p_{\rm T}}(p_{\rm T}) = \int_0^{2\pi} f_{p_{\rm T},\varphi}(p_{\rm T},\varphi){\rm d}\varphi, \tag{8}$$

and the φ distribution is

$$f_\varphi(\varphi) = \int_0^\infty f_{p_{\rm T},\varphi}(p_{\rm T},\varphi){\rm d}p_{\rm T}. \tag{9}$$

Similarly, the unit-density functions of p_z and $p_{\rm T}$ can be given by

$$\begin{aligned} & f_{p_z,p_{\rm T}}(p_z,p_{\rm T}) \\ =\ & f_{p_z}(p_z)f_{p_{\rm T}}(p_{\rm T}) \\ =\ & \frac{p_{\rm T}}{(2\pi)^{3/2}\sigma^3 a_x a_y a_z}\exp\left[-\frac{1}{2\sigma^2}\left(\frac{p_z-b_z\sigma}{a_z}\right)^2\right] \\ & \times\int_0^{2\pi}\exp\left[-\frac{1}{2\sigma^2}\left(\frac{p_{\rm T}\cos\varphi-b_x\sigma}{a_x}\right)^2\right. \\ & \left.-\frac{1}{2\sigma^2}\left(\frac{p_{\rm T}\sin\varphi-b_y\sigma}{a_y}\right)^2\right]{\rm d}\varphi. \end{aligned} \tag{10}$$

Considering the momentum

$$p=\sqrt{p_z^2+p_{\rm T}^2} \tag{11}$$

and the polar angle

$$\vartheta=\arctan\frac{p_{\rm T}}{p_z}, \tag{12}$$

the unit-density functions of p and ϑ are

$$\begin{aligned} & f_{p,\vartheta}(p,\vartheta) \\ =\ & pf_{p_z,p_{\rm T}}(p\cos\vartheta,p\sin\vartheta) \\ =\ & \frac{p^2\sin\vartheta}{(2\pi)^{3/2}\sigma^3 a_x a_y a_z}\exp\left[-\frac{1}{2\sigma^2}\left(\frac{p\cos\vartheta-b_z\sigma}{a_z}\right)^2\right] \\ & \times\int_0^{2\pi}\exp\left[-\frac{1}{2\sigma^2}\left(\frac{p\sin\vartheta\cos\varphi-b_x\sigma}{a_x}\right)^2\right. \\ & \left.-\frac{1}{2\sigma^2}\left(\frac{p\sin\vartheta\sin\varphi-b_y\sigma}{a_y}\right)^2\right]{\rm d}\varphi. \end{aligned} \tag{13}$$

The p distribution is

$$f_p(p)=\int_0^{\pi}f_{p,\vartheta}(p,\vartheta){\rm d}\vartheta, \tag{14}$$

and the ϑ distribution is

$$f_\vartheta(\vartheta)=\int_0^{\infty}f_{p,\vartheta}(p,\vartheta){\rm d}p. \tag{15}$$

In the Monte Carlo calculation, let R_1, R_2, R_3, R_4, R_5, and R_6 denote random variables distributed in $[0,1]$, we have

$$p'_{x,y,z}=\sqrt{-2\ln R_{1,3,5}}\cos(2\pi R_{2,4,6})\sigma, \tag{16}$$

because $p'_{x,y,z}$ obey the Gaussian distribution. From Eqs.(5) and (11), the transverse momentum and momentum are obtained as

$$p_{\rm T}=\sigma\sqrt{[a_x\sqrt{-2\ln R_1}\cos(2\pi R_2)+b_x]^2+[a_y\sqrt{-2\ln R_3}\cos(2\pi R_4)+b_y]^2} \tag{17}$$

and

$$p=\sqrt{p_{\rm T}^2+\sigma^2[a_z\sqrt{-2\ln R_5}\cos(2\pi R_6)+b_z]^2} \tag{18}$$

respectively. From Eqs.(6) and (12), the azimuthal and polar angles can be written as

$$\varphi=\arctan\frac{p_y}{p_x}=\arctan\frac{a_y\sqrt{-2\ln R_3}\cos(2\pi R_4)+b_y}{a_x\sqrt{-2\ln R_1}\cos(2\pi R_2)+b_x} \tag{19}$$

and

$$\vartheta=\arctan\frac{p_{\rm T}}{p_z}=\arctan\frac{\sqrt{[a_x\sqrt{-2\ln R_1}\cos(2\pi R_2)+b_x]^2+[a_y\sqrt{-2\ln R_3}\cos(2\pi R_4)+b_y]^2}}{a_z\sqrt{-2\ln R_5}\cos(2\pi R_6)+b_z} \tag{20}$$

respectively.

From the above discussion, we see that two methods both can be used to calculate the azimuthal and polar angle distributions. For convenience, we use the Monte Carlo method in this paper. The azimuthal and polar angle distributions can be obtained by a statistical method. An isotropic emission gives $a_{x,y,z}=1$ and $b_{x,y,z}=0$. The physics condition gives $a_{x,y,z}\geq 1$. The number and excitation degrees of emission sources do not affect the azimuthal and polar angles.

Because the parameters $b_{x,y,z}$ are normalized to the width of the momentum distribution, the expressions for φ and ϑ do not contain the parameter σ. This allows us to describe the particle angular distribution in a way that is independent of the temperature of the source. The parameters $B_{x,y,z}$ describe how much the

source is displaced from the beam axis or what the average transverse momentum of the source is, and the parameters $b_{x,y,z}$ describe only the displacement coefficient of the source. To obtain the temperature (or σ), one should use the distribution of transverse momentum $p_{\rm T}$, but not the azimuthal and polar angle distributions.

3. Comparison with experimental data

The left panels of Fig.1 show the π^+ (upper panel) and K^+ (lower panel) azimuthal distributions that are measured at the values of impact parameter b ranging

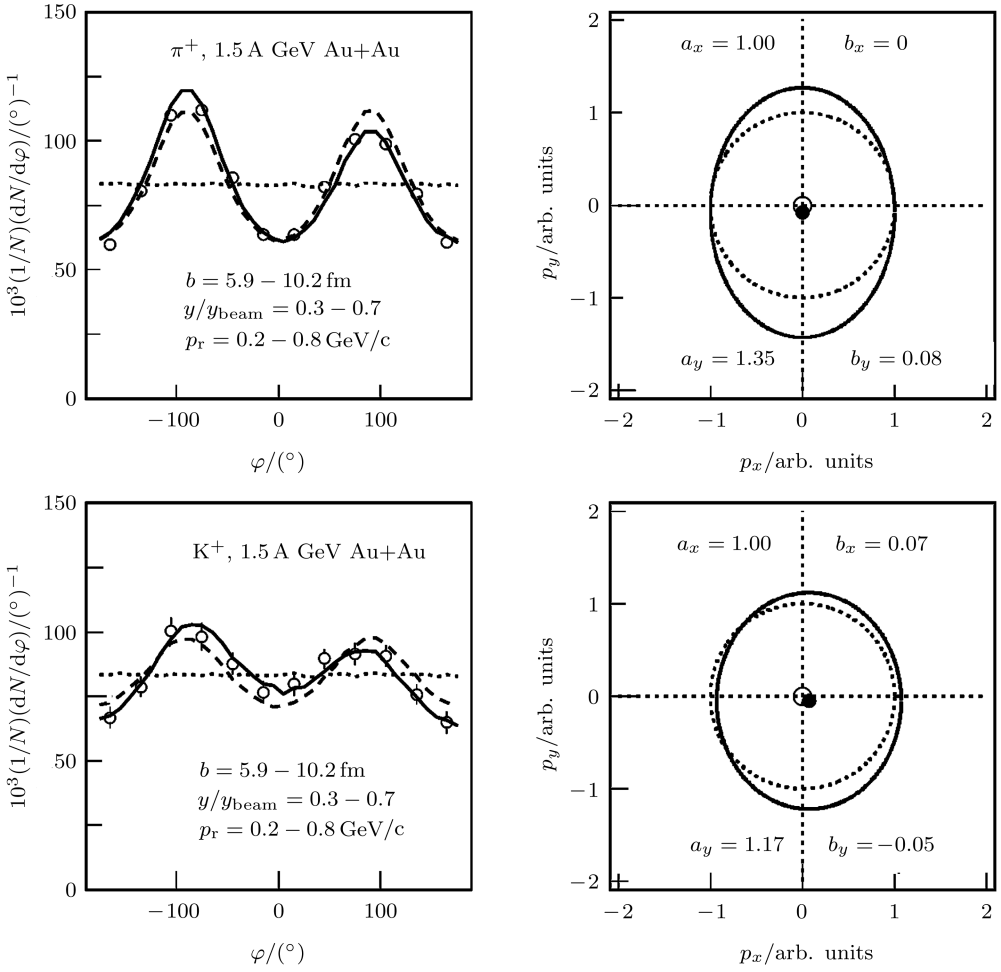


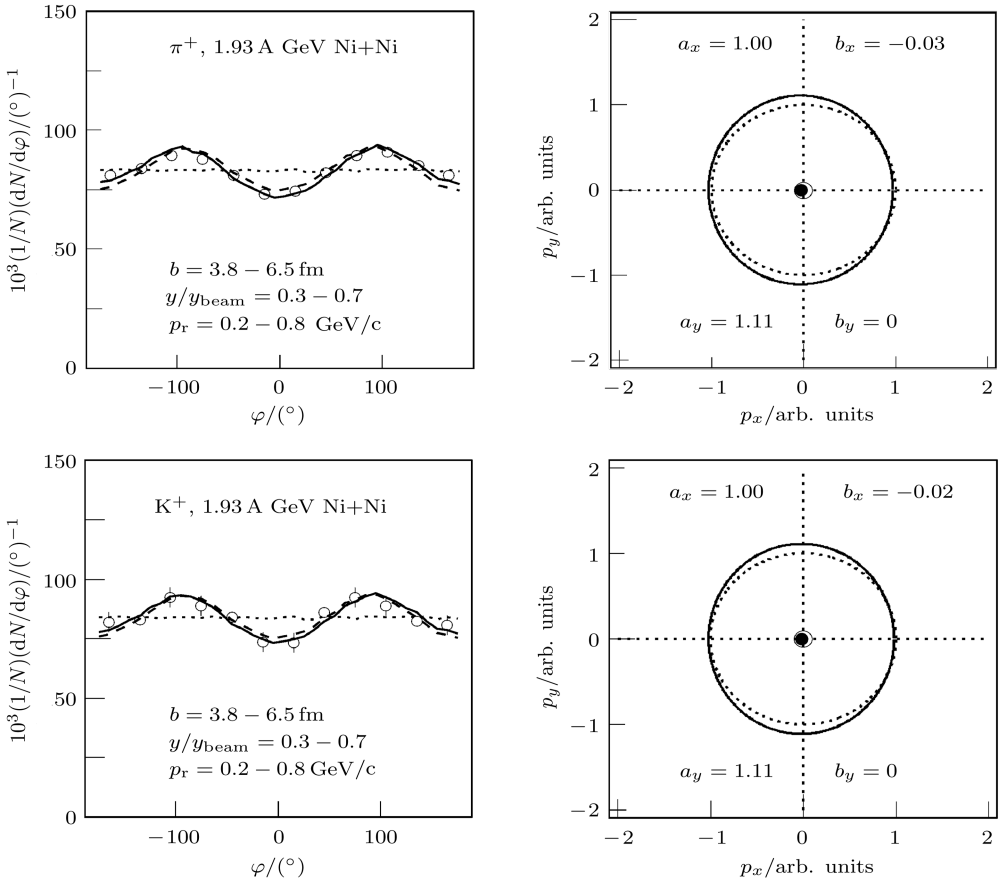
Fig.1. Left panels: Azimuthal distributions of π^+ (upper panel) and K^+ (lower panel) for the values of chosen impact parameter (b), rapidity over beam rapidity ($y/y_{\rm beam}$), and transverse momentum ($p_{\rm T}$) bins in Au–Au collisions at 1.5 A GeV. The circles denote the KaoS experimental data.[28,29] The continuous, dashed, and dotted curves represent our results calculated by using the Monte Carlo method. Right panels: Transverse structures of emission sources. The continuous curve circles represent the emission sources in the $p_x - p_y$ plane and correspond to the azimuthal distributions described by the continuous curves in the left panels. The dotted curve circles denote the normal isotropic source and correspond to the azimuthal distributions described by the dotted curves in the left panels. The dashed curves in the left panel refer to the calculated results with keeping $a_{x,y}$ unchanged and letting $b_{x,y} = 0$. The values of chosen b, $y/y_{\rm beam}$, $p_{\rm T}$ bins, $a_{x,y}$ and $b_{x,y}$, are shown in the figure.

from 5.9 to 10.2 fm, rapidity over beam rapidity $y/y_{\rm beam}$ from 0.3 to 0.7, and transverse momentum $p_{\rm T}$ from 0.2 to 0.8 GeV/c in Au–Au collisions at 1.5 A GeV, where N denotes the number of particles in the vertical axis direction. The circles refer to the KaoS experimental data.[28,29] The continuous curves represent our calculated results by using the Monte Carlo method, and the corresponding parameter values in

Eq.(19) for each event group are given in the right panels of Fig.1. The results without source expansion and movement are given in the left panels indicated by the dotted curves. To see the dependence of calculated results on the parameter values, the calculated results with keeping $a_{x,y}$ unchanged and letting $b_{x,y} = 0$ are indicated by the dashed curves in the figure. All calculations were done by using the Monte Carlo method, and for each case 10^6 particles were generated. In the calculation for the continuous curves, the χ^2-testing method was used. To see the shapes of the expansion and moving emission source in the momentum space in the transverse plane, which correspond to the continuous curves in the left panel, the continuous curve circles in the right panel represent the sources in the $p_x - p_y$ plane and the small full circles denote their centres. The dotted curve circles represent the original emission sources in the $p_x - p_y$ plane and the small open circles refer to their centres. Corresponding to the dotted curve circles in the right panels, the azimuthal distributions in the left panels are represented by the dotted curves. One can see an expansion of the source along the y-direction and a movement of the source along the negative y-direction for the emission of π^+, and an expansion of the source along the y-direction and a movement of the source along both the positive x- and negative y-directions for the emission of K^+.

The left panels of Fig.2 show the π^+ (upper panel), K^+ (middle panel), and K^- (lower panel) azimuthal distributions that are measured at the values of b ranging from 3.8 to 6.5 fm, $y/y_{\rm beam}$ from 0.3 to 0.7, and $p_{\rm T}$ 0.2 to 0.8 GeV/c in Ni–Ni collisions at 1.93A GeV. The circles denote the KaoS experimental data.[28,29] The meanings of curves in Fig.2 are the same as those in Fig.1. In 1.93 A GeV Ni–Ni collisions, one can see an expansion of the source along the y-direction and a movement of the source along the negative x-direction for both the emissions of π^+ and K^+, and an expansion of the source along the x-direction for the emission of K^-.

Given in the left panels of Fig.3 are the π^+ azimuthal distributions measured in the peripheral (upper panel) and semicentral (middle and lower panels) Au–Au collisions at 1 A GeV. For the three panels, the range of $y/y_{\rm beam}$ is 0.55–0.75. For the upper and middle panels, the values of $p_{\rm T}$ range from 0.26 to



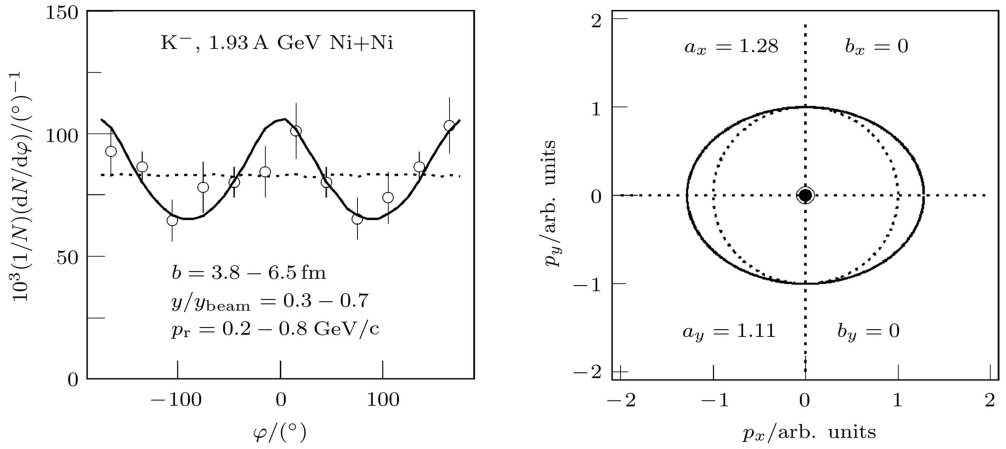
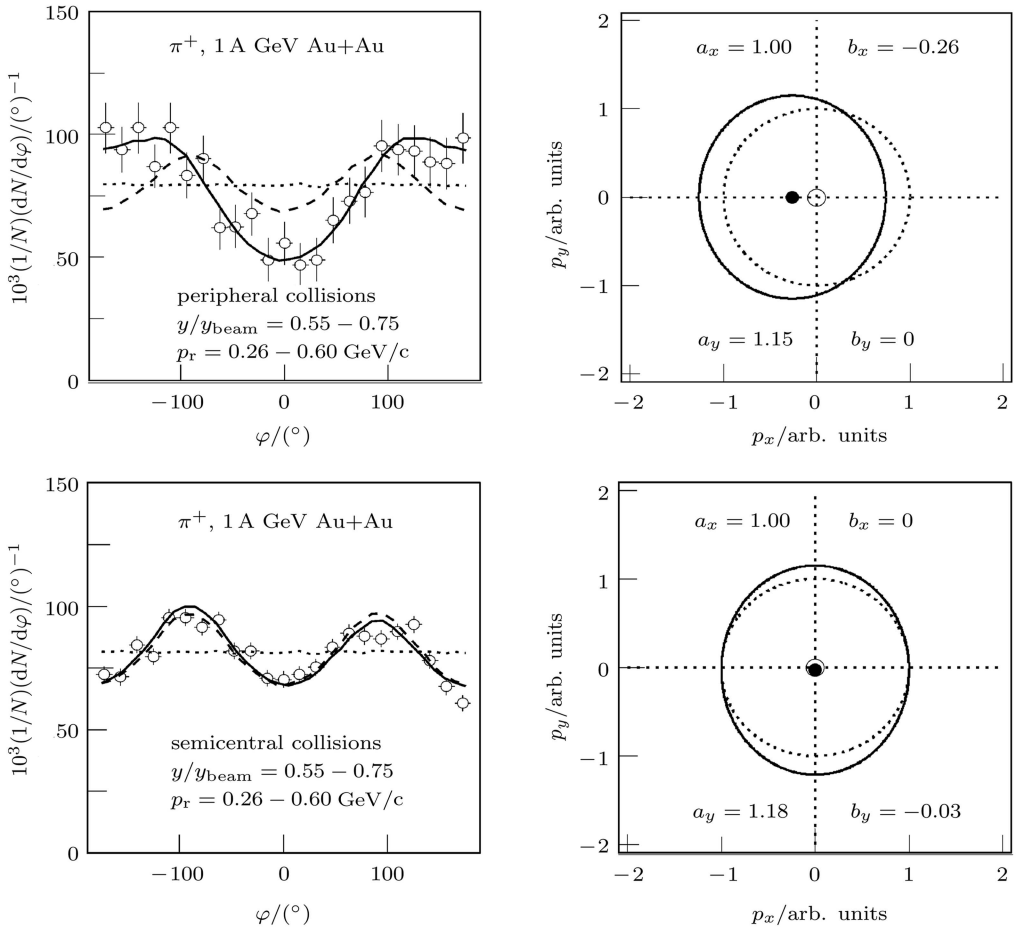


Fig.2. The description is the same as that for Fig.1, but it shows the results of π^+ (upper panel), K^+ (middle panel), and K^- (lower panel) in Ni–Ni collisions at 1.93A GeV. The experimental data are cited from Refs.[28,29].

0.60 GeV/c; and for the lower panel, the values of $p_{\rm T}$ are in a range of 0.16-0.26 GeV/c. The circles denote the KaoS experimental data.[30] The meanings of curves in Fig.3 are the same as those in Figs.1 and 2. In peripheral Au–Au collisions at 1 A GeV, one can see an expansion of the source along the y-direction and a movement of the source along the negative x-direction for the emission of π^+. In semicentral Au–Au collisions at 1A GeV, for the emission of π^+ at the values of $p_{\rm T}$ ranging from 0.26 to 0.60 GeV/c, one can see an expansion of the source along the y-direction and a movement of the source along the negative y-direction; and for the emission of π^+ at the values of $p_{\rm T}$ 0.16 to 0.26 GeV/c, one can see an expansion of the source along the y-direction and a movement of the source along the positive x-direction.



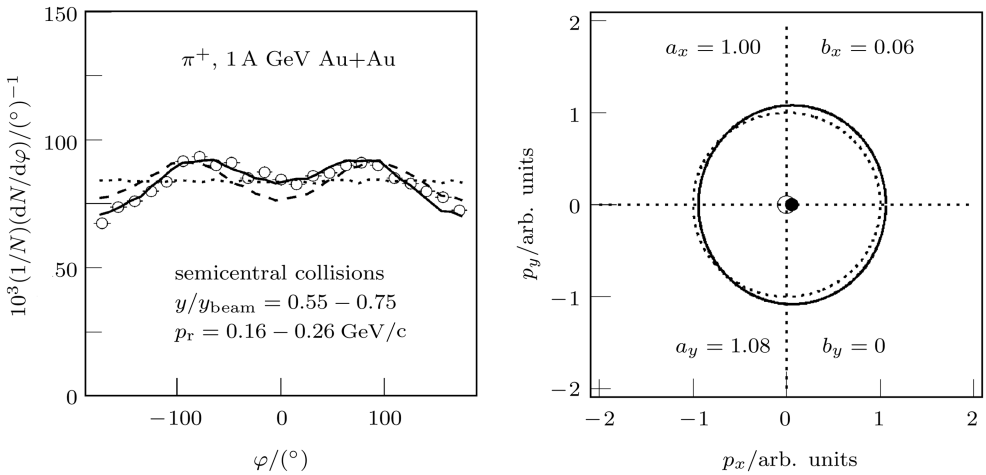
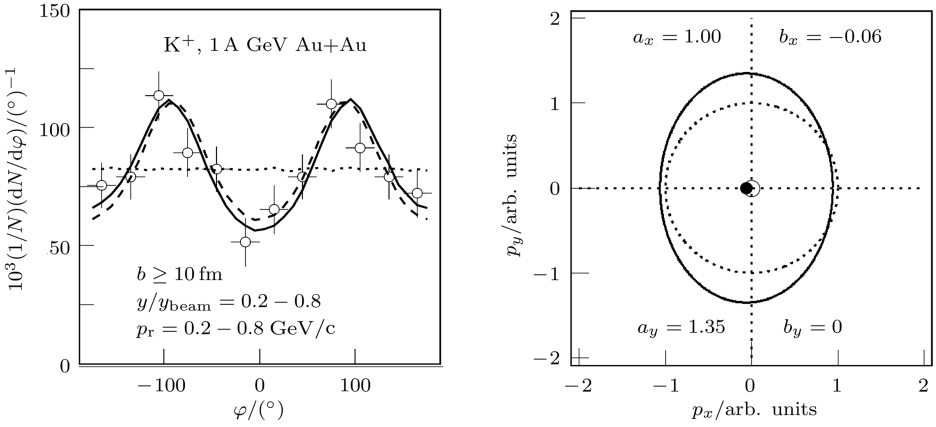


Fig.3. The description is the same as that for Fig.1, but it shows the results of π^+ in peripheral (upper panel) and semicentral (middle and lower panels) Au–Au collisions at 1A GeV. The experimental data are cited from Ref.[30].

Indicated in the left panels of Fig.4 are the K^+ azimuthal distributions that are measured in different event groups in Au–Au collisions at 1 A GeV. For the upper panel, $b \geq 10$ fm, and the values of $y/y_{\rm beam}$ range from and $p_{\rm T}$ 0.2 to 0.8, and from 0.2 to 0.8 GeV/c respectively; for the middle panel, the values of b,$y/y_{\rm beam}$ and $p_{\rm T}$ range from 5 to 10 fm, from 0.2 to 0.8, and from 0.2 to 0.8 GeV/c respectively; and for the lower panel, the values of b, $y/y_{\rm beam}$ and $p_{\rm T}$ range from 5 to 10 fm, from 0.4 to 0.6, and from 0.2 to 0.8 GeV/c. The circles refer to the KaoS experimental data.[31] The meanings of curves in Fig.4 are the same as those in Figs.1–3. For the emission of K^+ in Au–Au collisions at 1A GeV, in the case of $b \geq 10$ fm, one can see an expansion of the source along the y-direction and a movement of the source along the negative x-direction for the emission of K^+; and in the case of $b = 5 - 10$ fm, one can see an expansion of the source along the y-direction and a movement of the source along both the positive x- and negative y-directions.

The polar angle distributions of K^+ (upper panel) and K^- (lower panel) in non-central (left panel, $b >$ 6 fm) and near-central (right panel, $b <$ 6 fm) Au–Au collisions at 1.5 A GeV are shown in Fig.5, where $\vartheta_{\rm cm}$ on the axis denotes the polar angle in the centre-of-mass reference frame and $\sigma_{\rm inv}(\vartheta_{\rm cm})$ in the vertical axis represents the measured invariant production cross section of kaons with $\vartheta_{\rm cm}$. The full circles refer to the experimental data of the KaoS Collaboration and the open ones are the full circles reflected around $\cos\vartheta_{\rm cm} = 0$.[29] The continuous curves describe our results calculated by using the Monte Carlo method with the chosen a_z and b_z values shown in the figure. The dashed curves represent the Monte Carlo calculated results with keeping a_z unchanged and letting $b_z = 0$. The normal isotropic emission gives the results as shown in the figure by the dotted curves. In Au–Au collisions at 1.5 A GeV, one can see an expansion of the source along the z-direction and a movement of the projectile (target) source along the positive (negative) z-direction.



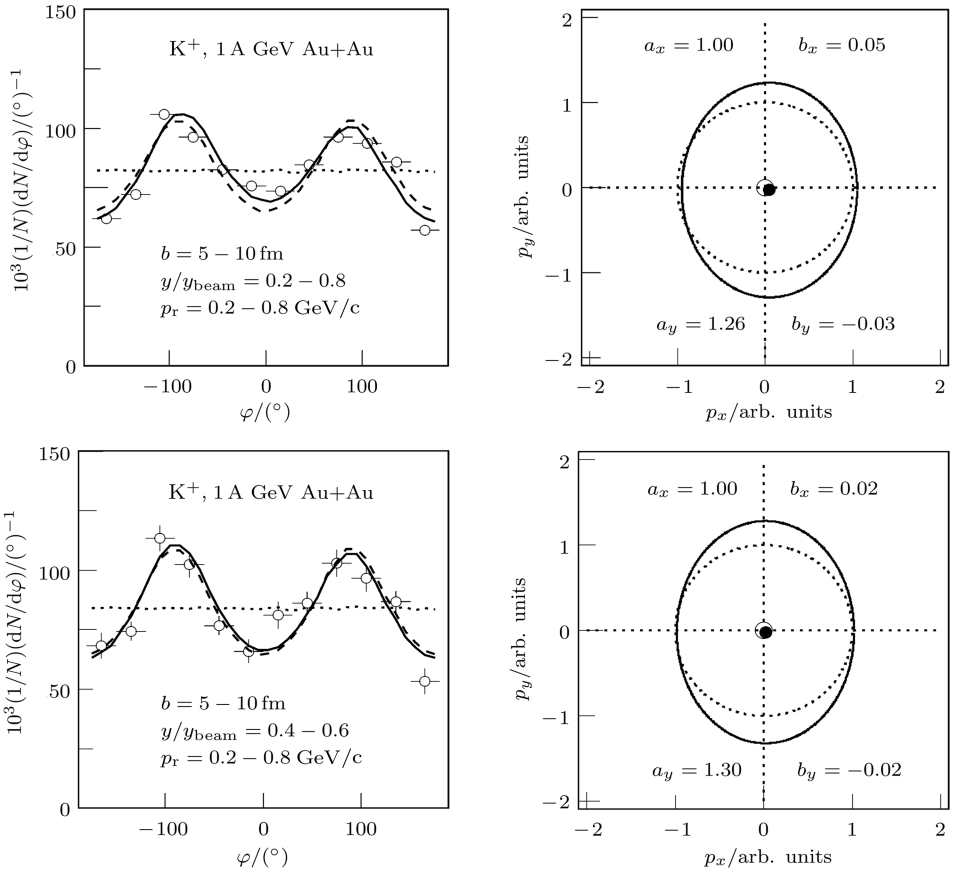
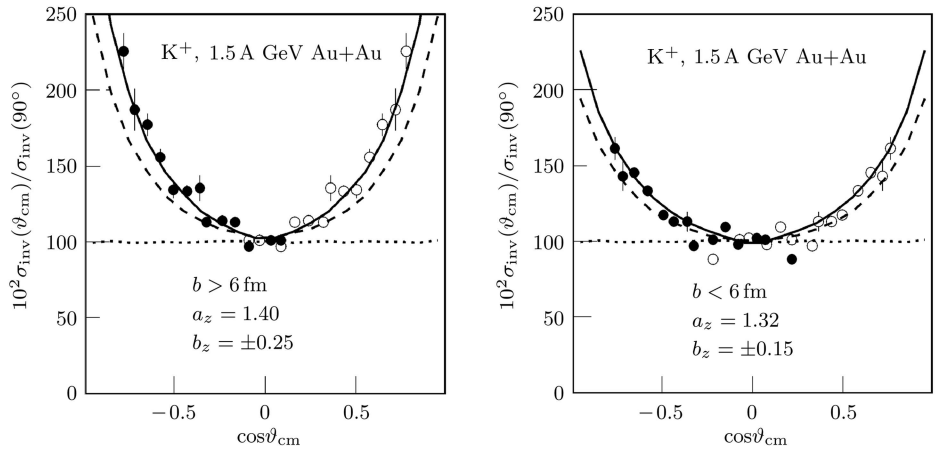


Fig.4. The description is the same as that for Fig.1, but it shows the results of K^+ in Au–Au collisions at 1 A GeV. The experimental data are cited from Ref.[31].

Figure 6 is similar to Fig.5, but it shows the polar angle distributions of K^+ (upper panel) and K^- (lower panel) in non-central (left panel) and near-central (right panel) Ni–Ni collisions at 1.93 A GeV. The full circles refer to the experimental data of the KaoS Collaboration and the open ones are the full circles reflected around $\cos\vartheta_{\rm cm} = 0$.[32] The meanings of curves are the same as those in Fig.5. In non-central Ni–Ni collisions at 1.93 A GeV, one can see an expansion of the source along the z-direction and a movement of the projectile (target) source along the positive (negative) z-direction. In near-central Ni–Ni collisions at 1.93 A GeV, one can see only a movement of the projectile (target) source along the positive (negative) z-direction.



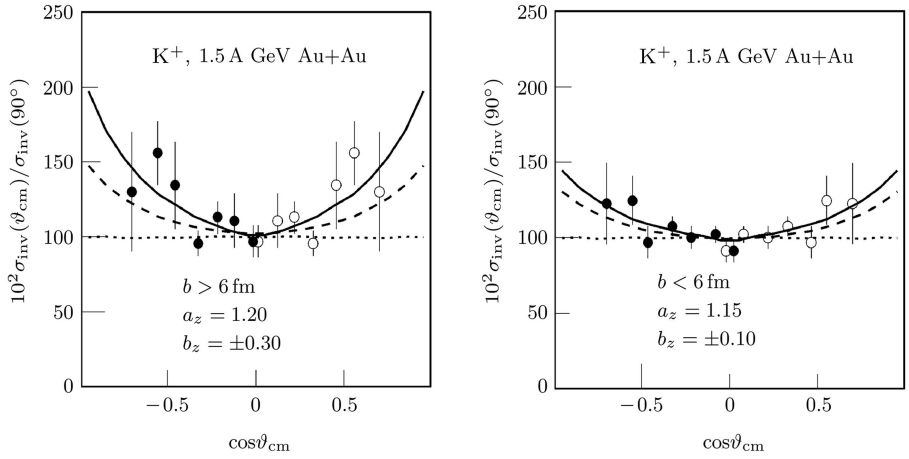


Fig.5. Polar angle distributions of K^+ (upper panel) and K^- (lower panel) in non-central (left panel, $b > 6$ fm) and near-central (right panel, $b < 6$ fm) Au–Au collisions at 1.5 A GeV. The full circles denote the experimental data of the KaoS Collaboration and the open ones are the full circles reflected around $\cos\vartheta_{cm} = 0$.[29] The continuous curves represent our results calculated by using the Monte Carlo method with the chosen a_z and b_z values shown in the figure. The dashed curves refer to the Monte Carlo calculated results with keeping a_z unchanged and letting $b_z = 0$. The normal isotropic emission gives the results shown in the figure by the dotted curves.

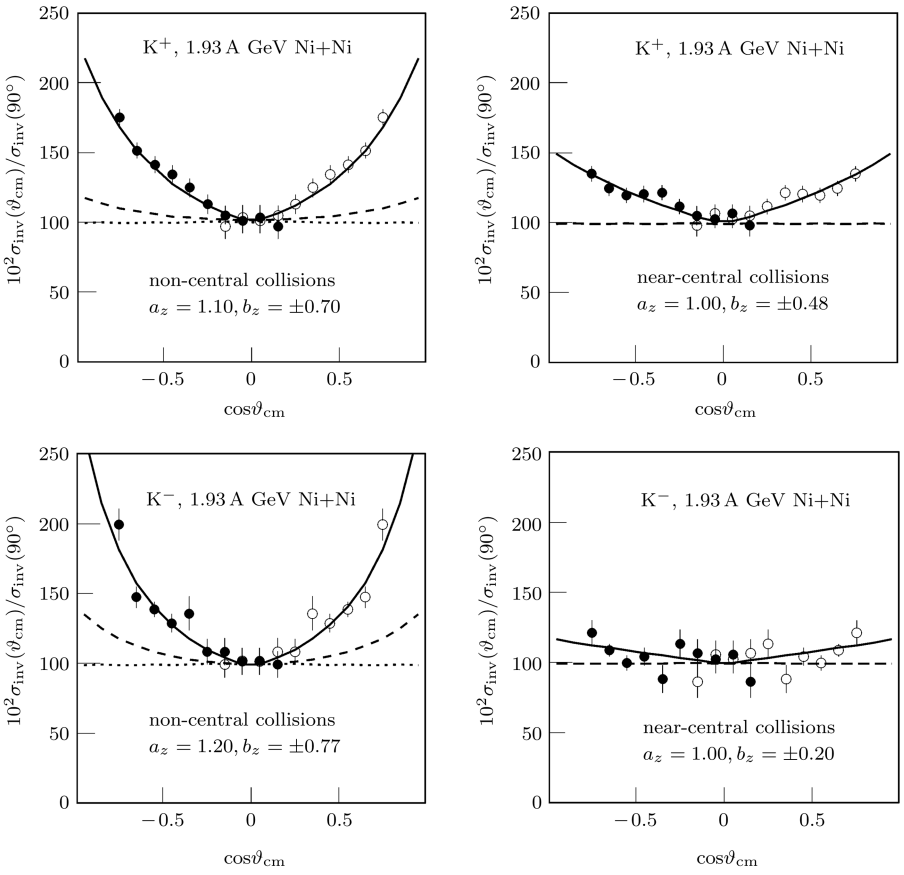


Fig.6. The description is the same as that for Fig.5, but it shows the polar angle distributions in non-central (left panel) and near-central (right panel) Ni–Ni collisions at 1.93 A GeV. The experimental data and their reflections are cited from Ref.[32].

4. Discussion and conclusion

In our previous work,[27] the meanings and the normal values of $a_{x,y}$ and $b_{x,y}$ were explained in terms of the transverse expansion and movement of the source in high energy heavy ion collisions, and the relation between the transverse (elliptic and directed) flows and the parameters ($a_{x,y}$ and $b_{x,y}$) was discussed. In the coordinate frame used in the present work, an in-reaction-plane transverse elliptic flow corresponds to $a_y > a_x \geq 1$ and the source has a relatively great expansion along the y-direction i.e. impact parameter direction, while an out-of-reaction-plane transverse elliptic flow corresponds to $a_x > a_y \geq 1$ and the source has a relatively great expansion along the x-direction (In Ref.[27], on in-plane and out-of-plane elliptic flows, it is regretful that we confused the relative sizes of a_x and a_y).

Similarly, a_z and b_z are expected to be related to the longitudinal (elliptic and directed) flows and can be explained in terms of the longitudinal structure of the source. $a_z > 1$ means an elliptic flow and the source having an expansion along the z-direction, while $a_z = 1$ means no flow and the source having no expansion. $b_z > 0$ (< 0) means a positive (negative) directed flow and the source having a movement along the positive (negative) z-direction, while $b_z = 0$ means no directed flow and the source having no movement along the z-direction. Generally speaking, the expansion and movement of the source are caused by the asymmetry of mechanics.

According to the above discussion, we can say that a mixture of an in-reaction-plane transverse elliptic flow and a transverse directed flow in x- or y- (or both x- and y-) directions is observed in azimuthal distributions of π^+ and K^+ in Au–Au and Ni–Ni collisions at 1–2 A GeV. From the azimuthal distribution of K^- produced in Ni–Ni collisions at 1.93 A GeV, we see an out-of-reaction-plane transverse elliptic flow. In non-central and near-central Au–Au collisions at 1.5 A GeV and non-central Ni–Ni collisions at 1.93 A GeV, we see a mixture of a longitudinal elliptic flow and a longitudinally directed flow from the $\cos\vartheta_{cm}$ distributions of kaons. For kaon production in near-central Ni–Ni collisions at 1.93 A GeV, a longitudinally directed flow is observed.

The present work concerns charged meson production in heavy ion collisions at the SIS energies. Our previous work[24−27] dealt with the emissions of final-state particles and fragments over an energy range covering the energies achieved by the AGS and SPS. It is interesting to test the multisource ideal gas model at higher and lower energies. Recently,[33] by using the multisource ideal gas model, we reconstructed the transverse emission source in the momentum space for light fragments with the values of mass number A being in a range of $1-4$ in reaction ^{86}Kr+^{124}Sn at 25 A MeV and large impact parameter ($b = 7-10$ fm) based on the theoretical predictions of the Isospin-Dependent Quantum Molecular Dynamics (IDQMD) model.[34] The parameters of the multisource ideal gas model were obtained by fitting the corresponding theoretical results of p_x distributions from the IDQMD model and meanwhile assuming that the emission source has no expansion and no movement along the y-direction. With these parameters and assumption, we have shown that the multisource ideal gas model can reasonably describe the IDQMD-predicted results for the azimuthal distribution and the $p_{\rm T}$ dependence of elliptic flow and fourth-order anisotropic flow, but it can only qualitatively describe the $p_{\rm T}$ spectra.[33] This implies that the multisource ideal gas model reasonably reproduces the relative deformation of the transverse emission source of the IDQMD model.[34]

We have investigated the azimuthal and polar angle distributions of pions and kaons produced in Au–Au and Ni–Ni collisions at 1–2A GeV. A multisource ideal gas model, which covers the expansions and movements of the source, gives a good description of the experimental data concerned. The formula obtained in the model can give the azimuthal and polar angle distributions directly, and the values of azimuthal and polar angles can be given by the Monte Carlo method, too. It is known that the azimuthal and polar angle distributions partly reflect the thermal properties of the interacting system. Our model shows that the normal isotropic thermal spectrum has an expansion and a movement in both the transverse and longitudinal momentum spaces. In the centre-of-mass reference frame, both the projectile and target sources have a movement in the longitudinal direction. In the Monte Carlo calculation, the formula is not related to the degree of excitation of the emission source, but it is based on the local equilibrium assumption.

References

[1] Senger P 2006 nucl-ex/0611010

[2] Sissakian A N, Sorin A S, Suleymanov M K, Toneev V D and Zinovjev G M 2005 nucl-ex/0511018

[3] Arndt R A, Briscoe W J, Strakovsky I I and Workman R L 2006 nucl-ex/0607014

[4] Xia J W, Rao Y N, Yuan Y J, Song M T, Yang X T, Yang X D, Liu S L, Zhao H W, Tang J Y, Zhan W L, Yuan P, Gu W, Wei W, Yano Y, Goto A, Katayama T and Watanabe S 1998 *Proceedings of the 1st Asian Particle Accelerator Conference* (APAC 1998), Tsukuba, Japan, 23–27 March

[5] Christakoglou P, Petridis A and Vassiliou M 2005 nucl-ex/0510045

[6] Lajoie J 2006 nucl-ex/0611002

[7] Dainese A 2005 *Czech. J. Phys.* **55** B367

[8] Adamovich M I, Aggarwal M M, Alexandrov Y A, Andreeva N P, Anzon Z V, Arora R, Avetian F A, Badyal S K, Basova E, Bhalla K B, Bhasin A, Bhatia V S, Bogdanov V G, Bubnov V I, Burnett T H, Cai X, Chasnikov I Y, Chernova L P, Chernyavsky M M, Eligbaeva G Z, Eremenko L E, Gaitinov A S, Ganssauge E R, Garpman S, Gerassimov S G, Grote J, Gulamov K G, Gupta S K, Gupta V, Heckman H H, Huang H, Jakobsson B, Judek B, Just L, Kachroo S, Kalyachkina G S, Kanygina E K, Karabova M, Kaul G L, Kitroo S, Kharlamov S P, Krasnov S A, Kulikova S, Kumar V, Lal P, Larionova V G, Lepetan V N, Liu L S, Lokanathan S, Lord J, Lukicheva N S, Luo S B, Maximkina T N, Mangotra L K, Marutian N A, Maslennikova N V, Mittra I S, Mookerjee S, Nasrulaeva H, Nasyrov S H, Navotny V S, Nystrand J, Orlova G I, Otterlund I, Palsania H S, Peresadko N G, Petrov N V, Plyushchev V A, Qarshiev D A, Qian W Y, Qin Y M, Raniwala R, Raniwala S, Rao N K, Rappoport V M, Rhee J T, Saidkhanov N, Salmanova N A, Sarkisova L G, Sarkisian V R, Shabratova G S, Shakhova T I, Shiplev S N, Skelding D, Soderstrom K, Soloveva Z I, Stenlund E, Surin E L, Svechnikova L N, Tolstov K D, Thotova M, Tretyakova M I, Trofimova T P, Tuleeva U, Vokal S, Wang H Q, Weng Z Q, Wilkes R J, Xia Y L, Xu G F, Zhang D H, Zheng P Y, Zhokhova S I and Zhou D C (EMU01 Collaboration) 1992 *Phys. Rev. Lett.* **69** 745

[9] Barrette J, Bellwied R, Bennett S, Braun-Munzinger P, Cleland W E, Cormier T M, David G, Dee J, Diebold G E, Dietzsch O, Fox D, Germani J V, Gilbert S, Greene S V, Hall J R, Hemmick T K, Herrmann N, Hong B, Jayananda K, Kraus D, Kumar B S, Lacasse R, Li Q, Lissauer D, Llope W J, Ludlam T W, McCorkle S, Majka R, Mark S K, Matheus R, Mitchell J T, Muthuswamy M, O'Brien E, Panitkin S, Pruneau C, Rao M N, Rosati M, Rotondo F, da Silva N C, Simon-Gillo J, Sonnadara U, Stachel J, Sullivan J, Takai H, Takagui E M, Throwe T G, Winter C, Wang G, Wolf K L, Wolfe D, Woody C L, Xu N, Zhang Y, Zhang Z and Zou C (E814/E877 Collaboration) 1993 *Phys. Rev. Lett.* **70** 2996

[10] Agakichiev G, Appelshauser H, Baur R, Braun-Munzinger P, Cherlin A, Drees A, Esumi S I, Filimonov K, Fraenkel Z, Fuchs C, Glassel P, Hering G, Lenkeit B, Marn A, Messer F, Messer M, Milosevic J, Miskowiec D, Nix O, Panebratsev Y, Petracek V, Pfeiffer A, Rak J, Ravinovich I, Razin S, Rehak P, Sako H, Saveljic N, Schmitz W, Shimansky S, Socol E, Slvova J, Specht H J, Stachel J, Tilsner H, Tserruya I, Voigt C, Voloshin S, Weber C, Wessels J P, Wurm J P and Yurevich V (CERES/NA45 Collaboration) 2004 *Phys. Rev. Lett.* **92** 032301

[11] Abelev B I, Aggarwal M M, Ahammed Z, Anderson B D, Anderson M, Arkhipkin D, Averichev G S, Bai Y, Balewski J, Barannikova O, Barnby L S, Baudot J, Bekele S, Belaga V V, Bellingeri-Laurikainen A, Bellwied R, Benedosso F, Bhardwaj S, Bhasin A, Bhati A K, Bichsel H, Bielcik J, Bielcikova J, Bland L C, Blyth S L, Bonner B E, Botje M, Bouchet J, Brandin A V, Bravar A, Burton T P, Bystersky M, Cadman R V, Cai X Z, Caines H, de la Barca Sanchez M C, Castillo J, Catu O, Cebra D, Chajecki Z, Chaloupka P, Chattopadhyay S, Chen H F, Chen J H, Cheng J, Cherney M, Chikanian A, Christie W, Coffin J P, Cormier T M, Cosentino M R, Cramer J G, Crawford H J, Das D, Das S, Dash S, Daugherity M, de Moura M M, Dedovich T G, DePhillips M, Derevschikov A A, Didenko L, Dietel T, Djawotho P, Dogra S M, Dong W J, Dong X, Draper J E, Du F, Dunin V B, Dunlop J C, Dutta Mazumdar M R, Eckardt V, Edwards W R, Efimov L G, Emelianov V, Engelage J, Eppley G, Erazmus B, Estienne M, Fachini P, Fatemi R, Fedorisin J, Filip P, Finch E, Fine V, Fisyak Y, Fu J, Gagliardi C A, Gaillard L, Ganti M S, Ghazikhanian V, Ghosh P, Gonzalez J E, Gorbunov Y G, Gos H, Grebenyuk O, Grosnick D, Guertin S M, Guimaraes K S, Gupta N, Gutierrez T D, Haag B, Hallman T J, Hamed A, Harris J W, He W, Heinz M, Henry T W, Hepplemann S, Hippolyte B, Hirsch A, Hjort E, Hoffman A M, Hoffmann G W, Horner M J, Huang H Z, Huang S L, Hughes E W, Humanic T J, Igo G, Jacobs P, Jacobs W W, Jakl P, Jia F, Jiang H, Jones P G, Judd E G, Kabana S, Kang K, Kapitan J, Kaplan M, Keane D, Kechechyan A, Khodyrev V Y, Kim B C, Kiryluk J, Kisiel A, Kislov E M, Klein S R, Kocoloski A, Koetke D D, Kollegger T, Kopytine M, Kotchenda L, Kouchpil V, Kowalik K L, Kramer M, Kravtsov P, Kravtsov V I, Krueger K, Kuhn C, Kulikov A I, Kumar A, Kuznetsov A A, Lamont M A, Landgraf J M, Lange S, LaPointe S, Laue F, Lauret J, Lebedev A, Lednicky R, Lee C H, Lehocka S, LeVine M J, Li C, Li Q, Li Y, Lin G, Lin X, Lindenbaum S J, Lisa M A, Liu F, Liu H, Liu J, Liu L, Liu Z, Ljubicic T, Llope W J, Long H, Longacre R S, Love W A, Lu Y, Ludlam T, Lynn D, Ma G L, Ma J G, Ma Y G, Magestro D, Mahapatra D P, Majka R, Mangotra L K, Manweiler R, Margetis S, Markert C, Martin L, Matis H S, Matulenko Y A, McClain C J, McShane T S, Melnick Y, Meschanin A, Millane J, Miller M L, Minaev N G, Mioduszewski S, Mironov C, Mischke A, Mishra D K, Mitchell J, Mohanty B, Molnar L, Moore C F, Morozov D A, Munhoz M G, Nandi B K, Nattrass C, Nayak T K, Nelson J M, Nepali N S, Netrakanti P K, Nogach L V, Nurushev S B, Odyniec G, Ogawa A, Okorokov V, Oldenburg M, Olson D, Pachr M, Pal S K, Panebratsev Y, Panitkin S Y, Pavlinov A I, Pawlak T, Peitzmann T, Perevoztchikov V, Perkins C, Peryt W, Phatak S C, Picha R, Planinic M, Pluta J, Poljak N, Porile N, Porter J, Poskanzer A M, Potekhin M, Potrebenikova E, Potukuchi B V, Prindle D, Pruneau C, Putschke J, Rakness G, Raniwala R, Raniwala S, Ray R L, Razin S V, Reinnarth J, Relyea D, Ridiger A, Ritter H G, Roberts J B, Rogachevskiy O V, Romero J L, Rose A, Roy C, Ruan L, Russcher M J, Sahoo R, Sakuma T, Salur S, Sandweiss J, Sarsour M, Sazhin P S, Schambach J, Scharenberg R P, Schmitz N, Seger J, Selyuzhenkov I, Seyboth P, Shabetai A, Shahaliev E, Shao M, Sharma M,

Shen W Q, Shimanskiy S S, Sichtermann E P, Simon F, Singaraju R N, Smirnov N, Snellings R, Sood G, Sorensen P, Sowinski J, Speltz J, Spinka H M, Srivastava B, Stadnik A, Stanislaus T D, Stock R, Stolpovsky A, Strikhanov M, Stringfellow B, Suaide A A, Subba N L, Sugarbaker E, Sumbera M, Sun Z, Surrow B, Swanger M, Symons T J, Szanto de Toledo A, Tai A, Takahashi J, Tang A H, Tarnowsky T, Thein D, Thomas J H, Timmins A R, Timoshenko S, Tokarev M, Trainor T A, Trentalange S, Tribble R E, Tsai O D, Ulery J, Ullrich T, Underwood D G, Van Buren G, van der Kolk N, van Leeuwen M, Vander Molen A M, Varma R, Vasilevski I M, Vasiliev A N, Vernet R, Vigdor S E, Viyogi Y P, Vokal S, Voloshin S A, Waggoner W T, Wang F, Wang G, Wang J S, Wang X L, Wang Y, Watson J W, Webb J C, Westfall G D, Wetzler A, Whitten J C, Wieman H, Wissink S W, Witt R, Wood J, Wu J, Xu N, Xu Q H, Xu Z, Yepes P, Yoo I K, Yurevich V I, Zhan W, Zhang H, Zhang W M, Zhang Y, Zhang Z P, Zhao Y, Zhong C, Zoulkarneev R, Zoulkarneeva Y, Zubarev A N and Zuo J X (STAR Collaboration) 2006 *Phys. Rev. Lett.* **97** 152301

[12] Adler S S, Afanasiev S, Aidala C, Ajitanand N N, Akiba Y, Al-Jamel A, Alexander J, Aoki K, Aphecetche L, Armendariz R, Aronson S H, Averbeck R, Awes T C, Babintsev V, Baldisseri A, Barish K N, Barnes P D, Bassalleck B, Bathe S, Batsouli S, Baublis V, Bauer F, Bazilevsky A, Belikov S, Bjorndal M T, Boissevain J G, Borel H, Brooks M L, Brown D S, Bruner N, Bucher D, Buesching H, Bumazhnov V, Bunce G, Burward-Hoy J M, Butsyk S, Camard X, Chand P, Chang W C, Chernichenko S, Chi C Y, Chiba J, Chiu M, Choi I J, Choudhury R K, Chujo T, Cianciolo V, Cobigo Y, Cole B A, Comets M P, Constantin P, Csana M, Cso T, Cussonneau J P, d'Enterria D, Das K, David G, Dea F, Delagrange H, Denisov A, Deshpande A, Desmond E J, Devismes A, Dietzsch O, Drachenberg J L, Drapier O, Drees A, Durum A, Dutta D, Dzhordzhadze V, Efremenko Y V, En'yo H, Espagnon B, Esumi S, Fields D E, Finck C, Fleuret F, Fokin S L, Fox B D, Fraenkel Z, Frantz J E, Franz A, Frawley A D, Fukao Y, Fung S Y, Gadrat S, Germain M, Glenn A, Gonin M, Gosset J, Goto Y, Granier de Cassagnac R, Grau N, Greene S V, Grosse Perdekamp M, Gustafsson H A, Hachiya T, Haggerty J S, Hamagaki H, Hansen A G, Hartouni E P, Harvey M, Hasuko K, Hayano R, He X, Heffner M, Hemmick T K, Heuser J M, Hidas P, Hiejima H, Hill J C, Hobbs R, Holzmann W, Homma K, Hong B, Hoover A, Horaguchi T, Ichihara T, Ikonnikov V V, Imai K, Inaba M, Inuzuka M, Isenhower D, Isenhower L, Ishihara M, Issah M, Isupov A, Jacak B V, Jia J, Jinnouchi O, Johnson B M, Johnson S C, Joo K S, Jouan D, Kajihara F, Kametani S, Kamihara N, Kaneta M, Kang J H, Katou K, Kawabata T, Kazantsev A V, Kelly S, Khachaturov B, Khanzadeev A, Kikuchi J, Kim D J, Kim E, Kim G B, Kim H J, Kinney E, Kiss A, Kistenev E, Kiyomichi A, Klein-Boesing C, Kobayashi H, Kochenda L, Kochetkov V, Kohara R, Komkov B, Konno M, Kotchetkov D, Kozlov A, Kroon P J, Kuberg C H, Kunde G J, Kurita K, Kweon M J, Kwon Y, Kyle G S, Lacey R, Lajoie J G, Le Bornec Y, Lebedev A, Leckey S, Lee D M, Leitch M J, Leite M A, Li X H, Lim H, Litvinenko A, Liu M X, Maguire C F, Makdisi Y I, Malakhov A, Manko V I, Mao Y, Martinez G, Masui H, Matathias F, Matsumoto T, McCain M C, McGaughey P L, Miake Y, Miller T E, Milov A, Mioduszewski S, Mishra G C, Mitchell J T, Mohanty A K, Morrison D P, Moss J M, Mukhopadhyay D, Muniruzzaman M, Nagamiya S, Nagle J L, Nakamura T, Newby J, Nyanin A S, Nystrand J, O'Brien E, Ogilvie C A, Ohnishi H, Ojha I D, Okada H, Okada K, Oskarsson A, Otterlund I, Oyama K, Ozawa K, Pal D, Palounek A P, Pantuev V, Papavassiliou V, Park J, Park W J, Pate S F, Pei H, Penev V, Peng J C, Pereira H, Peresedov V, Pierson A, Pinkenburg C, Pisani R P, Purschke M L, Purwar A K, Qualls J M, Rak J, Ravinovich I, Read K F, Reuter M, Reygers K, Riabov V, Riabov Y, Roche G, Romana A, Rosati M, Rosendahl S S, Rosnet P, Rykov V L, Ryu S S, Saito N, Sakaguchi T, Sakai S, Samsonov V, Sanfratello L, Santo R, Sato H D, Sato S, Sawada S, Schutz Y, Semenov V, Seto R, Shea T K, Shein I, Shibata T A, Shigaki K, Shimomura M, Sickles A, Silva C L, Silvermyr D, Sim K S, Soldatov A, Soltz R A, Sondheim W E, Sorensen S P, Sourikova I V, Staley F, Stankus P W, Stenlund E, Stepanov M, Ster A, Stoll S P, Sugitate T, Sullivan J P, Takagi S, Takagui E M, Taketani A, Tanaka K H, Tanaka Y, Tanida K, Tannenbaum M J, Taranenko A, Tarja P, Thomas T L, Togawa M, Tojo J, Torii H, Towell R S, Tram V N, Tserruya I, Tsuchimoto Y, Tydesjo H, Tyurin N, Uam T J, van Hecke H W, Velkovska J, Velkovsky M, Veszpre V, Vinogradov A A, Volkov M A, Vznuzdaev E, Wang X R, Watanabe Y, White S N, Willis N, Wohn F K, Woody C L, Xie W, Yanovich A, Yokkaichi S, Young G R, Yushmanov I E, Zajc W A, Zhang C, Zhou S, Zima J, Zolin L and Zong X (PHENIX Collaboration) 2006 *Phys. Rev. Lett.* **96** 222301

[13] Wang X N 1997 *Phys. Rep.* **280** 287

[14] Topor Pop V, Gyulassy M, Barrette J, Gale C, Wang X N and Xu N 2004 *Phys. Rev.* C **70** 064906

[15] Cunqueiro L, Ferreiro E G, del Moral F and Pajares C 2005 *Phys. Rev.* C **72** 024907

[16] Broniowski W, Hiller B, Florkowski W and Bozek P 2006 *Phys. Lett.* B **635** 290

[17] Ko C M 2006 *AIP Conf. Proc.* **828** 439

[18] Liu J Y, Guo W J, Ren Zh Zh, Xing Y Zh, Zuo W and Lee X G 2006 *Chin. Phys.* **15** 1738

[19] Yong G Ch, Li B A and Zuo W 2005 *Chin. Phys.* **14** 1549

[20] Zhang Y F, Huang Sh L, Zhang Z P and Wu J 2007 *Chin. Phys.* **16** 58

[21] Li Q, Jiang Zh J and Xia H F 2006 *Acta Phys. Sin.* **55** 5161 (in Chinese)

[22] Yong G Ch, Li B A, Chen L W and Zuo W 2006 *Acta Phys. Sin.* **55** 5166 (in Chinese)

[23] Bian B A, Zhou H Y and Zhang F Sh 2007 *Acta Phys. Sin.* **56** 1334 (in Chinese)

[24] Liu F H 2003 *Europhys. Lett.* **63** 193

[25] Liu F H, Abd Allah N N, Zhang D H and Duan M Y 2003 *Int. J. Mod. Phys.* E **12** 713

[26] Liu F H, Abd Allah N N and Singh B K 2004 *Phys. Rev.* C **69** 057601

[27] Liu F H, Ma Y Q and Duan M Y 2005 *Chin. Phys.* **14** 2458

[28] Uhlig F, Forster A, Bottcher I, Debowski M, Dohrmann F, Grosse E, Koczon P, Kohlmeyer B, Laue F, Menzel M, Naumann L, Oeschler H, Scheinast W, Schwab E, Senger P, Shin Y, Strobele H, Sturm C, Surowka G, Wagner A and Walus W (KaoS Collaboration) 2005 *Phys. Rev. Lett.* **95** 012301

[29] Forster A 2005 *J. Phys.* G **31** S693

[30] Brill D, Ahner W, Baltes P, Barth R, Bormann C, Cieslak M, Debowski M, Grosse E, Henning W, Koczon P, Kohlmeyer B, Miskowiec D, Muntz C, Oeschler H, Poppl H, Puhlhofer F, Sartorius S, Schicker R, Senger P, Shin Y, Speer J, Stein J, Stiebing K, Stock R, Strobele H, Volkel K, Wagner A and Walus W 1993 *Phys. Rev. Lett.* **71** 336

[31] Shin Y, Ahner W, Barth R, Beckerle P, Brill D, Cieslak M, Debowski M, Grosse E, Koczon P, Kohlmeyer B, Mang M, Miskowiec D, Muntz C, Oeschler H, Puhlhofer F, Schwab E, Schicker R, Senger P, Speer J, Strobele H, Sturm C, Volkel K, Wagner A and Walus W (KaoS Collaboration) 1998 *Phys. Rev. Lett.* **81** 1576

[32] Menzel M, Bottcher I, Debowski M, Dohrmann F, Forster A, Grosse E, Koczon P, Kohlmeyer B, Laue F, Naumann L, Oeschler H, Puhlhofer F, Schwab E, Senger P, Shin Y, Strobele H, Sturm C, Surowka G, Uhlig F, Wagner A and Walus W (KaoS Collaboration) 2000 *Phys. Lett.* B **495** 26

[33] Liu F H, Li J Sh and Duan M Y 2007 *Phys. Rev.* C **75** 054613

[34] Yan T Z, Ma Y G, Cai X Z, Chen J G, Fang D Q, Guo W, Ma C W, Ma E J, Shen W Q, Tian W D and Wang K 2006 *Phys. Lett.* B **638** 50